Nonlinear quantum magnetotransport in a strongly correlated two-dimensional electron liquid

Yu. P. Monarkha
Institute for Solid State Physics, University of Tokyo, Roppongi 7-22-1, Tokyo 106, Japan
and Institute for Low Temperature Physics and Engineering, 47 Lenin Avenue, 310164 Kharkov, Ukraine

K. Shirahama and K. Kono
Institute for Solid State Physics, University of Tokyo, Roppongi 7-22-1, Tokyo 106, Japan

F. M. Peeters
Department of Physics, University of Antwerp (UIA), B-2610 Antwerp, Belgium
(Received 24 October 1997)

Experimental and theoretical studies of nonlinear quantum magnetotransport of a nondegenerate two-dimensional electron liquid formed on the surface of liquid helium are reported. Measurements of the magnetoconductivity as a function of the input voltage are done using the edge magnetoplasmon (EMP) damping method. A nonlinear theory based on the many-electron self-consistent Born approximation (SCBA) is introduced to explain the data. It is shown that the nonlinear decrease of σ_{xx} observed at strong magnetic fields ($B \approx 3$ T) is due to the cold quantum nonlinear effect caused by the peaked structure of the electron density of states. At weak fields ($B \leqslant 1$ T), the heating effect competes with this effect and become of the same magnitude. The magnetic field dependence of the nonlinear narrowing of the EMP damping is in good agreement with the nonlinear many-electron SCBA. [S0163-1829(98)07728-5]

I. INTRODUCTION

Quantum magnetotransport in two-dimensional (2D) electron systems is of fundamental interest due to the singular nature of these systems in the presence of a strong magnetic field oriented normal to the 2D plane. The quantum Hall effect of degenerate 2D electrons in semiconductors[1,2] and the unusual magnetoconductivity behavior of nondegenerate 2D electrons on the surface of liquid helium[3,4] originate from the peaked structure of the electron density of states in strong magnetic fields.

It is known that in 2D electron systems the usual Born approximation leads to a magnetoconductivity $\sigma_{xx}=\infty$ for elastic scattering at static impurities, due to the fact that the electron encounters the same scatterer multiple times and the collision duration becomes effectively infinite.[5] The same approach for inelastic scattering within the lowest Landau level makes $\sigma_{xx}=0$ due to the δ-function structure of the unperturbed density of states. The generally accepted way of treating such a singular system is the self-consistent Born approximation (SCBA),[6] which takes into account the Landau level broadening due to the interaction with scatterers. In this case, the duration of the collision at impurities is proportional to the lifetime τ, or inversely proportional to the Landau level broadening $\Gamma=\hbar/\tau$, which results in a finite conductivity: $\sigma_{xx} \propto 1/\Gamma$. For inelastic scattering, the final result depends on the relation between the energy exchanged at a collision $\hbar\Delta\omega$ and the level broadening.[4,7] In the limiting case $\hbar\Delta\omega \ll \Gamma$, electron scattering can be approximately treated as elastic.

In a nondegenerate electron system like surface electrons (SE) on helium, the linear magnetotransport is rather unusual. In the ultraquantum limit, for both kinds of scatterers available in this system (vapor atoms and capillary wave quanta or ripplons) the effective collision frequency of electrons $\nu(B)$ increases faster with the magnetic field B than the cyclotron frequency ω_c. This means that the Hall angle or the sideways motion of electrons decreases with increasing magnetic field; a behavior that is opposite to the classical Hall effect. For vapor atom scattering at rather high temperatures $T>1.5$ K, this unusual behavior makes the high cyclotron frequency approximation ($\omega_c \gg \nu$ or $\sigma_{xx} \simeq e^2 n \nu(B)/m\omega_c^2$, here n is the electron density and m is the free electron mass) inapplicable in the limit of strong magnetic fields. In Refs. 3 and 8 the extended SCBA was introduced to describe the unusual Hall effect. In this theory, the SCBA is formulated for the effective collision frequency $\nu(B)$, which determines quantum magnetotransport by means of elementary equations for the conductivity tensor. For low electron densities, the extended SCBA perfectly describes the experimental data up to $B \approx 20$ T.

Another unexpected behavior of σ_{xx} appears at low temperatures where the electron-ripplon scattering dominates. According to Ref. 4, the energy exchanged at a collision, $\hbar\omega_q$, increases with the magnetic field B faster than the Landau-level broadening Γ, due to the unusual ripplon dispersion $\omega_q \propto q^{3/2}$, which breaks the elastic approximation ($\hbar\omega_q \ll \Gamma$) previously used in the single-electron[9] and many-electron[10] theories of quantum magnetotransport of SE on helium.

The remarkable properties of SE on superfluid helium allows the Landau level broadening Γ to satisfy the unique condition $\Gamma \ll k_B T \ll \hbar\omega_c$. According to Ref. 11, under this condition, new nonlinear magnetotransport phenomena may occur without heating of the electron system ($T_e \simeq T$). These phenomena are of pure quantum nature, since they are caused by the narrow peaked structure of the density of states and therefore can be used for experimental studies of the

many-body properties of a 2D electron liquid in quantizing magnetic fields.

Physically, the cold nonlinear magnetotransport effect can be explained as follows. For example, consider electron scattering on helium vapor atoms, which can be treated like elastic scattering on static impurities, since the time duration that an atom spends within the electron orbit of radius $l=\sqrt{\hbar c/eB}$ is much larger than the orbit lifetime τ. In the presence of a driving electric field $E_{\|}$, the drift of an electron orbit with velocity $\mathbf{u}$ can reduce the amount of multiple scattering on the same scatterer, if the time duration which an electron spends near the impurity $\tau_{\mathrm{dr}}=l/u$ becomes shorter than $\tau=\hbar/\Gamma$. As the basic linear magnetoconductivity properties of a 2D electron system is caused by multiple encounters of the same scatterer, this effect reduces both σ_{xx} and Γ.

The cold nonlinear effect can also be explained in another way, which is more appropriate for electron-ripplon scattering, which is analogous to electron-phonon scattering in solids. Strongly correlated SE are in equilibrium in the center-of-mass frame, which moves with the drift velocity $\mathbf{u}$. Relative to this frame, impurities (vapor atoms) and ripplons move with the velocity $-\mathbf{u}$ in the opposite direction, and the energy transfer between an electron and a scatterer (even for electron-impurity scattering) can no longer be neglected. The additional energy exchanged at a single collision $\hbar\Delta\omega=\hbar\mathbf{q}\cdot\mathbf{u}$ (here $\hbar\mathbf{q}$ is momentum transfer) can be inconsistent with the Landau-level width, if $|\hbar\Delta\omega|>\Gamma$. For both kinds of scattering $q\simeq 1/l$ which makes the two nonlinear criteria found here ($\tau_{\mathrm{dr}}<\hbar/\Gamma$ and $\hbar|\mathbf{q}\cdot\mathbf{u}|>\Gamma$) equivalent. Therefore the effect can also be considered as the nonlinear breakdown of the elastic approximation.

In general, both the cold nonlinear effect and the heating effect appear to be of the same importance for the SE on helium, due to the relatively low-energy relaxation rate of the electron system. The energy collision frequency ν_{en} is approximately three or four orders of magnitude lower than the momentum collision frequency ν. To reduce heating and to observe the quantum nonlinear effect in a real experiment with SE, we use the edge magnetoplasmon (EMP) method of measuring the conductivity σ_{xx} described in Refs. 4 and 12. According to this method, σ_{xx} is found from the EMP damping coefficient. In this case, the very narrow strip of SE near the edge of the electron pool is heated and absorbs energy from the electric field. At the same time, due to the very short electron-electron autocorrelation time, the electron temperature T_e is the same within the whole electron sheet and all electrons take part in the energy relaxation. Thus the effective energy collision frequency that enters the energy balance equation increases by approximately one order of magnitude, which makes heating practically negligible at strong magnetic fields.

Preliminary experimental results showing the nonlinear narrowing of the EMP damping were reported in Refs. 12 and 13 for the ripplon scattering regime.

In this paper, we present a detailed experimental study of nonlinear quantum magnetotransport of highly correlated SE on helium by means of the EMP damping method (Sec. II). To interpret the data, we develop the nonlinear many-electron SCBA theory (Sec. III). As a probe for the many-electron SCBA, the limit of linear quantum magnetotransport is analyzed and compared with available experimental data and the results of previous theoretical approaches (Sec. IV). The nonlinear analysis presented here (Sec. IV B) proves that the narrowing of the SE magnetoconductivity with increasing amplitude of the input voltage observed at strong magnetic fields and at low temperatures can be perfectly understood in terms of the quantum cold nonlinear effect.

II. EXPERIMENT

Here besides the considerable reduction of heating, which is important for studying the cold nonlinear effect, the EMP damping method serves as an alternative to the capacitive coupling technique in the Corbino geometry. The latter proved to be quite effective for measuring σ_{xx} at relatively high temperatures where the vapor atom scattering dominates. At low temperatures and strong magnetic fields the Corbino technique requires many precautions to avoid the excitation of EMP waves, which causes spuriousness in the experimental data. Such waves are excited due to small deviations of the system from axial symmetry or a slight tilt. The EMP damping method used here is immune to asymmetry, and consequently the excitation of EMP waves is an excellent tool for studying the quantum magnetotransport of SE at low temperatures.

In the EMP wave,[14,15], which propagates along the edge of the electron pool, charge density fluctuations are localized only near the edge within a characteristic width a. At strong magnetic fields, a is the width of the transition region, where the electron density changes smoothly from zero to its bulk value n.

The electron sheet in the present work has a circular geometry with radius R_{el}, which is shaped by an assembly of electrodes. The inner electrode is 10 mm in radius, which is surrounded by four outer electrodes that are identical and arc shaped. The outer radius of the assembly is 15 mm. The assembly is situated $d\approx 1.0$ mm under the liquid helium surface. A numerical study of the charge distribution profile gives $a\approx 0.3$ mm. The electron density n was estimated from the depth of the liquid helium and the applied dc voltage. The experiment was carried out under saturated electron density conditions with fixed $n=3.5\times 10^7$ cm^{-2}.

The cell containing the electrodes is mounted on a dilution refrigerator. Resistance thermometry was employed to measure temperature. At low temperatures the resistance thermometers have been calibrated from the ^{3}He melting curve. Although the thermometers are not inside the cell, we found that the temperature difference between the thermometer and the sample is negligible, which we concluded from the fact that no hysteresis was found in a temperature sweep up and down.

The EMP is excited by an ac voltage of frequency ω applied to one of the outer electrodes. The voltage induced by the EMP is detected on the opposite end. The resonance is observed by sweeping the frequency of the ac voltage. The signal analyzed by a two-phase lock-in emerges as a typical resonance curve. The basic resonance $m=1$ is somewhat noisy (see Ref. 4) and there is a low-frequency distortion, which is due to the usual Hall effect. Therefore we mostly used the $m=2$ resonance to perform the analysis. This choice does not affect the conductivity results, since practically the same damping coefficient was found for the third

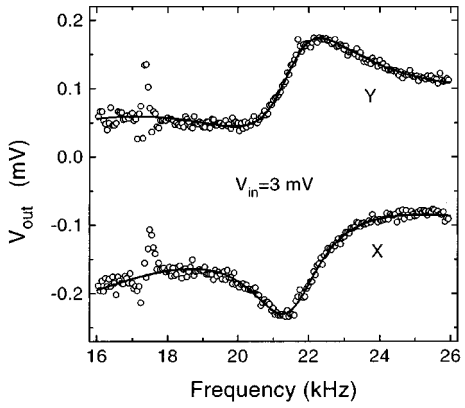

FIG. 1. The experimental signal from the biphase lock-in amplifier (X: in-phase, Y: out-of-phase) as a function of frequency for $T=0.3$ K, $n=3.5\times10^7$ cm^{-2}, and $B=1.8$ T. Solid curves represent the results obtained by fitting to Lorentzians.

and fourth resonances, in accordance with the basic concept of EMP waves.

The resonance frequency ω_m and the damping coefficient $1/\tau_m$ are obtained by fitting the observed resonance curve to the following formula based on the Lorentzian line shape,

$$Y(\omega;C_0,C_1,C_2,\Delta\tau,\omega_m,\tau_m) = \left[C_0+C_1\omega+\frac{C_2}{\omega_m^2-\omega^2+2i\omega/\tau_m}\right]e^{i\omega\Delta\tau}, \quad (1)$$

where $\Delta\tau$, ω_m, and $1/\tau_m$ are real parameters, whereas C_0, C_1, and C_2 are complex ones. The exponential factor in Eq. (1) takes into account the delay, $\Delta\tau$, of the signal because of the electronic circuit. The terms containing C_0 and C_1 eliminate the baseline offset, which could arise from the influence of resonances with other m numbers. Fitting was done iteratively. Typical resonance graphs of the output signal and the fitting curves are shown in Fig. 1.

According to Ref. 16, the EMP damping is

$$\frac{1}{\tau_{\rm EMP}}\sim\sigma_{xx}\frac{\int_a^\infty E^2dy}{\Phi(a)Q}, \quad (2)$$

where E and Φ are the electric field and potential of the EMP respectively which are both proportional to the linear charge density Q accumulated near the edge. In the case of strong magnetic fields (practically at $B>0.1$ T), the parameter a is equal to the electron density transition width which is independent of B and T. Therefore at fixed electron density the EMP damping is proportional to σ_{xx}. This conclusion is in accordance with the detailed theoretical analysis of Ref. 17. The proportionality coefficient depends on the particular geometry of the experimental cell and the real shape of the electron density at the edge.

Aiming mainly at studying the ripplon dominated regime, we fixed the proportionality coefficient between σ_{xx} and $1/\tau_m$ at $T=1.1$ K where the ripplon contribution is negligible and the vapor atom scattering is well understood. We used a Drude formula at $B=0.294$ T with the zero-field mobility determined independently. Then the conductivity obtained from the EMP damping is in agreement with the theoretical and experimental results of Refs. 18 and 19.

EMP waves of the 2D electron liquid are excited by an ac voltage $V_{\rm in}$ applied to one of the outer electrodes. Thus the external ac electric field, $\mathbf{E}_\parallel^{(0)}=-\nabla\Phi^{(0)}$, is mostly localized near the gap between two neighboring electrodes and can be estimated as $V_{\rm in}/d$, where d is the helium depth. The real electric field responsible for EMP damping, $\mathbf{E}_\parallel=-\nabla\Phi$, is produced by electron density perturbations δn. In general, it is very difficult to find a direct relation between this field $E_\parallel$ and $V_{\rm in}$. Nevertheless it is possible to establish the frequency and magnetic field dependencies of the proportionality coefficient between $E_\parallel$ and $V_{\rm in}$, which we employ when comparing our experimental data and theory. For this purpose we use the qualitative analysis of the EMP dispersion introduced in Ref. 16 (an analogous method was also described in Ref. 20).

Employing the model of straight boundary (EMP waves propagate along the x direction, and the gap between two neighboring electrodes is along the y direction), the EMP dispersion equation, $(\omega-\omega_{\rm EMP})Q=0$, can be found combining the continuity equation $i\omega Q\approx j_y(y\sim a)$ and the equation for the current density at strong fields ($\sigma_{yx}\gg\sigma_{xx}$)

$$j_y\simeq\sigma_{yx}\partial\Phi/\partial x. \quad (3)$$

The potential of the EMP wave Φ is proportional to Q with a geometrical factor dependent on a. If we take into account that the external potential $\Phi^{(0)}$ should be added to Φ at the right-hand side of Eq. (3), then the relation between Q and $V_{\rm in}$ can be written as

$$Q\propto\frac{\sigma_{yx}}{\omega-\omega_{\rm EMP}}V_{\rm in}, \quad (4)$$

We found the same result by employing a more detailed analysis of the continuity equation and boundary condition for the current density proposed in Ref. 20.

At the resonant condition $\omega-\omega_{\rm EMP}\to0$, the denominator of Eq. (4) should be replaced by $1/\tau_{\rm EMP}\propto\sigma_{xx}$ and the relation between the amplitude of the electric field in the EMP wave and the applied voltage can be written as

$$E_\parallel\propto\frac{\sigma_{yx}}{\sigma_{xx}}V_{\rm in}. \quad (5)$$

Since the driving electric field in the EMP wave depends on σ_{xx}, according to Eq. (5), the nonlinear narrowing of the EMP damping is proportional to the nonlinear change of the SE conductivity only for sufficiently small nonlinear changes. This condition is characterized by the linear relation between $E_\parallel$ and $V_{\rm in}$. Strong nonlinear effects produce more rapid narrowing of the EMP damping than the real change of σ_{xx}, which we observe.

The approximation (1) is strictly valid only in the linear regime. In the nonlinear regime [$\sigma_{xx}(E_\parallel)\neq$const], the EMP damping becomes frequency dependent and the resonance curves lose their Lorentzian shapes due to $E_\parallel\propto Q$ and Eq. (4). Typical amplitude of the output signal is shown in Fig. 2 for different drive levels. For small nonlinear changes, to which

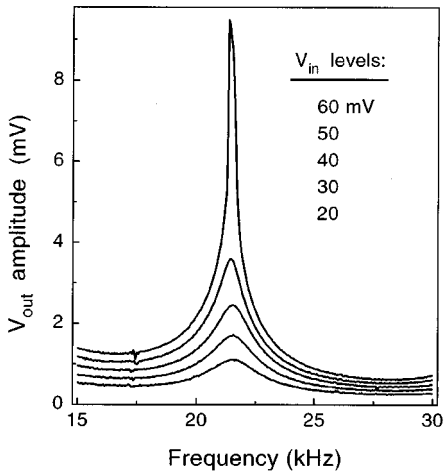

FIG. 2. The amplitude of the experimental signal as a function of the frequency for different input voltages. The lowest curve corresponds to the smallest value of $V_{\rm in}$. Experimental conditions are the same as in Fig. 1.

we mainly confine our experimental study, the correction to σ_{xx} is proportional to $-E_{\|}^2$ and the nonlinear effect can be described by the replacement

$$\gamma_m \equiv \frac{1}{\omega_m \tau_m} \rightarrow \gamma_{\rm lin} - (\gamma_{\rm lin} - \gamma_{\rm res}) \frac{\gamma_{\rm lin}^4}{(\epsilon^2 + \gamma_{\rm lin}^2)^2}$$

in the usual Lorentzian function $R(\epsilon) = \gamma_m / (\epsilon^2 + \gamma_m^2)$. Here $\epsilon = (\omega - \omega_m)/\omega_m$, $\gamma_{\rm lin}$ is the normalized linear EMP damping $1/(\omega_m \tau_m)$ or half-width of the linear resonance curve, and $\gamma_{\rm res}$ represents the EMP damping at the resonant condition $\epsilon = 0$.

Figure 3 shows the nonlinear resonance curves of the frequency-dependent width (FDW) model presented above for different levels of the nonlinear effect described by $\gamma_{\rm res} \leqslant \gamma_{\rm lin}$. In this model the difference $\gamma_{\rm lin} - \gamma_{\rm res}$ is a measure of the nonlinear effect. It is seen that the FDW model describes quite effectively the nonlinear narrowing of the EMP resonances. The nonlinear effect observed makes the resonance curves narrower and higher mostly at the vicinity of the maximum, while the tails remain unchanged, in accordance with the FDW model. It means that the physics of the nonlinear EMP resonances is well understood.

Thus, in the nonlinear regime, the experimental signals should be fitted to the FDW Lorentzians introduced above with an additional parameter $\gamma_{\rm res}$ representing σ_{xx} at $\omega = \omega_m$. Still it should be pointed out that the conventional fitting of the nonlinear curves reproduces $\gamma_{\rm res}$ remarkably well as a half-width of the usual Lorentzian function with $\gamma_{\rm fit}(\omega) = {\rm const}$, as was proven in Fig. 3 for the FDW model.

The electric field of the EMP wave rapidly falls beyond the edge strip, where the charge density is accumulated. It allows one to estimate the number of SE that are heated as $\Delta N_e \simeq 2aN_e/R_{\rm el}$. In our experiment we have $R_{\rm el} \approx 15$ mm and $a \approx 0.3$ mm. These numbers are used in the energy balance equation to estimate the electron temperature T_e.

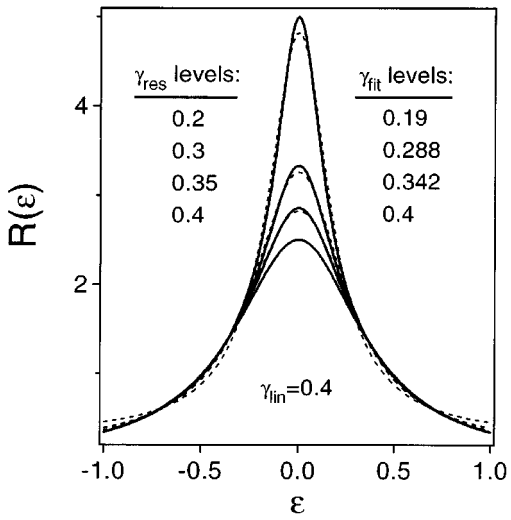

FIG. 3. The nonlinear resonance curves from the FDW model described in the text (solid curves) for different strengths of the nonlinear effect, $\gamma_{\rm lin} - \gamma_{\rm res}$. The lowest curve corresponds to the linear regime $\gamma_{\rm res} = \gamma_{\rm lin} = 0.4$. The dashed curves represent the result of fitting to Lorentzians with a frequency-independent half-width $\gamma_{\rm fit}$.

III. THEORY

Contrary to the SCBA theory, the single-electron (Saitoh[9]) and many-electron [Dykman and Khazan[10] (DK)] theories of quantum magnetotransport are more elaborate and are free of the problem of sharp Landau level wings. Nevertheless when applied to the real experimental conditions, these theories have difficulties. The theory of Ref. 9 did not take into account the Coulomb interaction between the electrons, which is very important at low temperatures. The DK theory includes the effect of mutual interaction on the electron density of states but disregards the level broadening that is caused by scatterers. Both theories disregard the inelastic effect important at strong magnetic fields.[4]

In Refs. 19 and 21 the DK theory was combined with SCBA by means of the well known Einstein diffusion formula. Unfortunately, the self-consistent procedure introduced in these papers was based on results that were proven for the case where only one kind of scatterer is present and, therefore, is not strictly correct, when there are additional causes for the level broadening such as mutual Coulomb interaction (the procedure is revised in Secs. III C and IV A).

The nonlinear as well as the inelastic reduction of σ_{xx} depends on the total broadening of the Landau level, which includes *both* the many-electron effect and the effect of scatterers. In this paper, we describe the nonlinear and inelastic effects in the frame of the many-electron SCBA theory. This approach allows one to treat the Coulomb broadening of the electron density of states in the same way as for the impurity scattering, which in our opinion is more appropriate than combining DK theory with SCBA. The approach is physically consistent and very instructive. At the same time, it appears to be quite effective for describing experimental data, providing one with theoretical results within the accuracy of 13% at least. We assume that the detailed behavior of the density of states at the wings of the Landau level is not important under the condition $k_{\rm B}T \gg \Gamma$ and the final result

does not depend much on the particular shape for the Landau level. We prove this assumption by employing different kinds of Landau-level shapes.

We use an extended version of the SCBA established for a highly correlated electron liquid.[3,8] This approach is similar to the momentum balance equation method[22] used for describing high-field magnetoresistance in semiconductor 2D electron systems. In comparison with the version of Refs. 3 and 8 we incorporated the many-electron and nonlinear effects.

A. Basic notations

The scattering of SE on helium vapor atoms dominates for $T>1$ K, while for sufficiently low temperatures $T<0.7$ K, it can be neglected as compared to the electron-ripplon scattering. Both kinds of scattering of SE can be described in a similar way by means of the interaction Hamiltonian represented as follows:

$$H_{\rm int}=\sum_{j=a,r}\sum_{\mathbf{q}} U_j n_{-\mathbf{q}} A_{j,\mathbf{q}}, \quad n_{\mathbf{q}}=\sum_e \exp(-i\mathbf{q}\cdot\mathbf{r}_e), \tag{6}$$

where the subscript $j=a$ corresponds to vapor atom scattering, and $j=r$ corresponds to electron-ripplon scattering. The many-body operators for ripplons $A_{r,\mathbf{q}}=b_{\mathbf{q}}+b^{\dagger}_{-\mathbf{q}}$ have the usual form ($b^{\dagger}_{\mathbf{q}}$ is the creation operator). In the case of electron-atom scattering, it is convenient to introduce operators $A_{a,\mathbf{q}}$ that have similar properties and that represent a sort of projection of the 3D vapor atom system onto the plane of the 2D electron system

$$A_{a,\mathbf{q}}=\sum_k \eta_k \sum_{\mathbf{K}'} a^{\dagger}_{\mathbf{K}'-\mathbf{K}} a_{\mathbf{K}'}, \tag{7}$$

where $\mathbf{K}=\{\mathbf{q},k\}$ is a 3D wave vector, $\eta_k=\langle 1|e^{ikz}|1\rangle$, $\langle 1||1\rangle$ means an average over the ground surface level, and $a^{\dagger}_{\mathbf{K}}$ is the creation operator of ^{4}He atoms.

The interaction parameters U_j entering Eq. (6) are defined as

$$U_r=V_q\sqrt{\frac{\hbar q}{2\rho\omega_q}}, \quad U_a=\frac{2\pi\hbar^2 s_0}{m}, \tag{8}$$

where V_q is the electron-ripplon coupling[23] whose detailed form will be presented in Sec. IV B, ρ is the liquid helium mass density, ω_q is the ripplon dispersion, m is the electron mass, and s_0 is the electron-atom scattering length.

The influence of the strong magnetic field on the electron system will be described in terms of Fermi creation and destruction operators of Landau level states $|N,X\rangle$

$$n_{\mathbf{q}}=\sum_X \sum_{NN'} J_{NN'}(\mathbf{q}) c^{\dagger}_{N,X} c_{N',X-l^2 q_y}, \tag{9}$$

with the matrix element $J_{NN'}=\langle N,X|\exp(-i\mathbf{q}\cdot\mathbf{r})|N',X-q_y l^2\rangle$.

Thus vapor atoms represent a nearly ideal example of short-range scatterers ($s_0\ll l$) convenient for the description of basic magnetotransport phenomena in 2D electron systems. Contrary to vapor atoms, ripplons are long-range scatterers, like phonons in solids. The matrix element $|J_{NN'}|^2$ is proportional to $\exp(-q^2l^2/2)$, and restricts the wave vectors to $q\leqslant\sqrt{2}/l$. An additional restriction $\hbar\omega_q\leqslant\Gamma$ appears due to the inelastic effect.

B. Nonlinear collision frequency concept

We consider an infinitely large isotropic 2D electron liquid moving along the helium surface in the presence of crossed magnetic $\mathbf{B}$ and electric $\mathbf{E}_{\|}$ fields. In the center-of-mass frame, moving with the drift velocity $\mathbf{u}$, the frequency of ripplons may be negative $\omega'_q=\omega_q-\mathbf{q}\cdot\mathbf{u}<0$, due to the unusual dispersion of the ripplons $\omega_q=\sqrt{\alpha/\rho}q^{3/2}$ (α is the surface tension). It should be noted that negative frequencies appear even in the linear theory for small enough q, which means physically that perturbations reach a supersonic observer in the reverse order. Still, the negative frequencies make the boson distribution function negative in the momentum balance equation method of Ref. 22. To avoid this unphysical quantity, we use another version of the momentum balance equation method introduced in Refs. 3,8 for the case of linear magnetotransport.

In the Born approximation, the momentum loss per second and the kinetic friction $\mathbf{F}_{\rm fr}$ can be found as a function of the dynamic structure factor (DSF) $S(\mathbf{q},\omega)=N_e^{-1}\int e^{i\omega t}\langle n_{\mathbf{q}}(t)n_{-\mathbf{q}}(0)\rangle dt$ of the 2D electron liquid in the fixed frame,

$$\mathbf{F}_{\rm fr}=\frac{N_e}{\hbar}\sum_{\mathbf{q}}\mathbf{q}\cdot\left\{U_a^2\sum_k|\eta_k|^2\sum_{\mathbf{K}'}N^{(a)}_{\mathbf{K}'}S(\mathbf{q},\Delta\omega_a)+U_r^2N^{(r)}_q[S(\mathbf{q},\omega_q)+\exp(\hbar\omega_q/k_{\rm B}T)S(\mathbf{q},-\omega_q)]\right\},$$

where $N^{(\mathbf{a})}_{\mathbf{K}'}$ and $N^{(\mathbf{r})}_{\mathbf{q}}$ are the distribution functions of vapor atoms and ripplons, respectively, N_e is the total number of SE, $\hbar\Delta\omega_a=\mathcal{E}^{(a)}_{\mathbf{K}'}-\mathcal{E}^{(a)}_{\mathbf{K}'-K}$ is the energy exchanged at the electron-atom collisions.

We assume that the strongly correlated electron system is in equilibrium in the center-of-mass frame, which leads to the relation $S(\mathbf{q},\omega)=S_0(q,\omega-\mathbf{q}\cdot\mathbf{u})$ in the fixed frame, where S_0 is the equilibrium DSF. Physically, it means that collective excitations of the moving electron system like 2D plasmons, which are responsible for a singularity in the DSF, has a dispersion affected by the Doppler shift $\omega_{p,\mathbf{q}}=\omega^{(0)}_{p,q}+\mathbf{q}\cdot\mathbf{u}$ in the fixed frame. This approximation is the quantum analog of the semiclassical treatment of strongly correlated electrons by means of the drift velocity shifted distribution function $f_{\mathbf{k}}=f(E-\hbar\mathbf{k}\cdot\mathbf{u})$. In semiconductor systems, this approximation is quite common though it requires the condition $\nu_{ee}\gg\nu$ (here ν_{ee} is the electron-electron autocorrelation frequency), which is difficult to realize. Contrary to the semiconductor systems, for SE on helium the condition $\nu_{ee}\gg\nu$ is fulfilled at low temperatures, and therefore the approximation is expected to be even numerically correct.

Using the well-known properties of the equilibrium DSF $S_0(q,-\omega)=e^{-\hbar\omega/k_BT_e}S_0(q,\omega)$ and the condition $\hbar\omega_q \ll k_BT$, the kinetic friction can be rewritten as

$$\mathbf{F}_{\rm fr}=\frac{N_e}{\hbar}\sum_{\mathbf{q}}\ \mathbf{q}\cdot\left[1-\exp\left(\frac{\hbar\mathbf{q}\cdot\mathbf{u}}{k_BT_e}\right)\right]\left[U_r^2N_q^{(r)}S_0(\mathbf{q},\omega_q-\mathbf{q}\cdot\mathbf{u})+\frac{1}{2}U_a^2\sum_k\ |\eta_k|^2\sum_{\mathbf{K}'}\ N_{\mathbf{K}'}^{(a)}S_0(\mathbf{q},\Delta\omega_a-\mathbf{q}\cdot\mathbf{u})\right]. \tag{10}$$

The Doppler energy correction $\hbar\mathbf{q}\cdot\mathbf{u}$ enters Eq. (10) by means of two different parameters $\hbar\mathbf{q}\cdot\mathbf{u}/k_BT_e$ and $\hbar\mathbf{q}\cdot\mathbf{u}/\Gamma$. The last one appears in the argument of the DSF due to the singular nature of the electron density of states. Taking into account that $\Gamma \ll k_BT$, we can expand the friction as a function of the small parameter $\hbar\mathbf{q}\cdot\mathbf{u}/k_BT_e$ while keeping the argument of the DSF.

In the treatment proposed above, from the force balance equation we obtain the components of the conductivity tensor [or the resistivity tensor $\rho_{xx}=m\nu(B,u)/ne^2$, $\rho_{xy}=B/nec$] in which the effective collision frequency $\nu(B,u)$ depends on the magnetic field, drift velocity, and electron temperature [here $\mathbf{F}_{\rm fr}=-N_em\nu(B,u)\mathbf{u}$]

$$\nu(B,u)=\frac{1}{mk_BT_e}\sum_{\mathbf{q}}\ q_u^2\left\{U_r^2N_q^{(r)}S_0(q,\omega_q-\mathbf{q}\cdot\mathbf{u})+\frac{1}{2}U_a^2\sum_k\ |\eta_k|^2\sum_{\mathbf{K}'}\ N_{\mathbf{K}'}^{(a)}S_0(q,\Delta\omega_a-\mathbf{q}\cdot\mathbf{u})\right\}. \tag{11}$$

A significant simplification of the nonlinear transport theory appears to be possible at sufficiently low temperatures ($T<1.5$ K) where $\sigma_{xx}\ll\sigma_{yx}$. In this case, Eq. (11) gives directly the driving field dependence of the transport coefficients caused by the cold nonlinear effect, if we take into account that $u\simeq eE_\parallel/m\omega_c$. At the same time, the electron temperature T_e is determined by the energy balance equation.

Thus the magnetotransport problem is now reduced to the determination of the equilibrium DSF of a 2D electron liquid in the presence of a strong magnetic field. It is instructive to note that for an ideal 2D electron gas in the limit of $u\to 0$, Eq. (11) and $\sigma_{xx}\simeq e^2n\nu(B)/m\omega_c^2$ lead to the results of the center migration approach and SCBA theory applied to the nondegenerate system of surface electrons.[24,25] At low temperatures, especially in the ripplon dominated scattering regime, SE represents a strongly correlated system in which the mean potential energy is approximately 100 times larger than the mean kinetic energy. Therefore, the ideal gas approximation of the DSF should be corrected. However, it should be pointed out that in the limit of strong magnetic fields $q\simeq 1/l\propto\sqrt{B}\to\infty$, the DSF of a 2D electron liquid is close to the DSF of an ideal electron gas, according to the results of numerical studies.[26]

Following Ref. 27, we assume that the many-electron effect produces an additional broadening of the electron density of states and therefore can be taken into account as a correction to the single-electron Green's function $G_N(E)$. In this treatment, using notations of Eq. (9), the DSF can be written as

$$S_0(q,\omega)=\frac{2\hbar}{\pi^2N_el^2}\int dE f(E)[1-f(E+\hbar\omega)]\times\sum_{N,N'}\ |J_{N,N'}|^2{\rm Im}G_N(E){\rm Im}G_{N'}(E+\hbar\omega), \tag{12}$$

where $f(E)$ is the Fermi-distribution function.

In the SCBA theory, the semielliptic Landau-level shape,

$$-{\rm Im}G_N(E)=\frac{2}{\Gamma_N}\sqrt{1-\left(\frac{E-E_N}{\Gamma_N}\right)^2}, \tag{13}$$

is found as a solution of the self-consistent equations for the single-electron Green's function. The cumulant expansion method of Ref. 28 yields the Gaussian Landau-level shape with the same broadening. This shape has the appropriate physical behavior at the edges of the Landau levels. In the simplified method,[28] the half ellipses of SCBA are replaced by Gaussians in the conductivity equations. The real Landau-level shape in fact is a mixture of an elliptic and a Gaussian form.[29]

In the ultraquantum limit ($N=0$, $\Gamma_0\equiv\Gamma$) and $\Gamma\ll k_BT$, Eqs. (12) and (13) yield

$$S_0(q,\omega)\simeq\frac{32\hbar}{3\pi\Gamma}\exp\left(-\frac{q^2l^2}{2}\right)Y_S\left(\frac{\hbar\omega}{\Gamma}\right), \tag{14}$$

with

$$Y_S(y)=\frac{3}{4}\int_{-1}^{1-y}\sqrt{1-x^2}\sqrt{1-(x+y)^2}dx\,\theta(2-|y|),$$

where $\theta(x)$ is the unit step function. Numerically, we found that $Y_S(y)$ is very close to the function $Y_G(y)=(3\pi^{3/2}/16)\exp(-y^2)$, as what one would find for the Gaussian Landau-level shape. Therefore, in contrast to the case of a degenerate 2D electron gas, the DSF for nondegenerate electrons is nearly independent of the used Landau-level shape, if $\Gamma\ll k_BT$. In the elastic theory the difference between $Y_S(0)$ and $Y_G(0)$ is less than 5%, which explains why the SE magnetoconductivity equations found for the semielliptic and Gaussian level shapes[3] are numerically so close to each other.

Dynamic correlations of SE in the presence of a quantizing magnetic field are confined to the very narrow energy scale $\sim\Gamma$, which is in contrast to the semiclassical treatment where k_BT is the only energy parameter entering the DSF of a nondegenerate 2D electron gas.[26] As mentioned in the Introduction, the nonlinear transport of strongly correlated nondegenerate 2D electrons should be treated as inelastic even when there is only impurity scattering and no internal states of an impurity are excited at a collision. Though the

total (averaged) energy transfer to the static impurities equals zero, the significant energy exchange between an electron and an impurity in a single collision appears for the electron center-of-mass frame due to the high drift velocity **u**. Therefore, the frequency dependence of DSF is the most important quantity for the description of the inelastic and nonlinear effects.

C. Dynamic correlations and level broadening

The single-electron Green's function entering Eq. (12) is assumed to be calculated in the center-of-mass frame, relative to which the vapor atoms and the ripplons are moving with the drift velocity $-\mathbf{u}$ in the opposite direction. The additional time-dependent factor $\exp(i\mathbf{q}\cdot\mathbf{u}t)$ that appears in the interaction Hamiltonian (6) can be taken into account by determining the ripplon and vapor gas operators $A_{j,\mathbf{q}}$ in the center-of-mass frame $A'_{j,\mathbf{q}}(t)=\exp(i\mathbf{q}\cdot\mathbf{u}t)\cdot A_{j,\mathbf{q}}(t)$.

The perturbation theory for the single-electron Green's function operates with the correlators

$$D_j(q,t-t')=-i\langle T[A_{j,\mathbf{q}}(t)A_{j,-\mathbf{q}}(t')]\rangle, \tag{15}$$

which are written in a similar way for both kinds of electron scattering ($j=a,r$). In the center-of-mass frame, we have $D_j(q,\omega)=D_j^{(0)}(q,\omega+\mathbf{q}\cdot\mathbf{u})$, which describes the Doppler shift for the perturbation source moving with the velocity $-\mathbf{u}$. Finally, the electron self-energy can be written as

$$\Sigma_N(E)=i\sum_{\mathbf{q}}\sum_{N'}|J_{N,N'}|^2\int\frac{d\omega}{2\pi}G_{N'}(E-\hbar\omega)\sum_j U_j^2 \times D_j^{(0)}(q,\omega+\mathbf{q}\cdot\mathbf{u}). \tag{16}$$

It should be noted that the result is the same, if we would evaluate Σ_N in the fixed frame and use the Doppler shift in the electron Green's function instead of in D_j.

In the argument of the electron Green's function (16), the frequency term $\hbar\omega$ is equal to the energy exchanged at a collision including the Doppler shift correction. If this term is much smaller than the typical electron energy scale, $E\sim\Gamma$, then we can disregard it as well as the mixing of the different Landau levels (it is also assumed that $\Gamma\ll\hbar\omega_c$). This yields

$$\Sigma_N(E)=\tfrac{1}{4}\Gamma_N^2 G_N(E), \tag{17}$$

where $\Gamma_N=\sqrt{\Gamma_{a,N}^2+\Gamma_{r,N}^2}$ is the total broadening, $\Gamma_{a,N}$ and $\Gamma_{r,N}$ are the level broadening induced by vapor atoms and ripplons, respectively. Consequently, contributions to Γ_N^2 from different scatterers are independent and Eq. (17) provides us with the rule of how to combine them to the total broadening Γ_N. Equation (17) together with the Dyson equation can be solved in a self-consistent way following Ref. 6, which results in the semielliptic Landau-level shape.

According to the general treatment of the Coulomb effect as presented in Ref. 27, the Landau levels will be additionally broadened due to the many-electron fluctuating electric field E_f for the same reason as it was due to the random impurity potential. The fluctuating electric field is produced in the center-of-mass frame, which means that there is no additional time-dependent factor $\exp(i\mathbf{q}\cdot\mathbf{u}t)$ in this case. It allows one to find the Coulomb contribution to the electron self-energy in the elastic way as $\frac{1}{4}\Gamma_{\mathrm{C},N}^2 G_N(E)$. Here $\Gamma_{\mathrm{C},N}$ is the broadening of the electron density of states produced by the mutual Coulomb interaction. For the ground level ($N=0$) Γ_{C} can be estimated as the electron energy uncertainty due to the fluctuating field $\Gamma_{\mathrm{C}}\approx eE_f l$ (the same estimate was used in Ref. 21). To be strict, we use the numerical proportionality factor $b\approx 1$ in the equation

$$\Gamma_{\mathrm{C}}=beE_f l, \quad E_f=0.84\sqrt{4\pi k_{\mathrm{B}}T_e n^{3/2}}, \tag{18}$$

where the fluctuating electric field was taken from the numerical simulations of Ref. 18.

In the elastic treatment, the total electron self-energy including the Coulomb correction can be written in the same way as Eq. (17) with the total broadening

$$\Gamma=\sqrt{\Gamma_a^2+\Gamma_r^2+\Gamma_{\mathrm{C}}^2}. \tag{19}$$

This result shows that the simple sum of different kinds of broadening as previously used in Ref. 19 in order to obtain the total broadening is not correct and can differ from the strict result by a factor of $\sqrt{2}$. More importantly, as the magnetic field increases, the sum of collision broadening and the many-electron effect of Ref. 19 approaches much more slowly the single-particle SCBA result than for $\Gamma=\sqrt{\Gamma_a^2+\Gamma_{\mathrm{C}}^2}$ according to the many-electron SCBA.

It is instructive to note that in the elastic regime there is no need for an additional self-consistent procedure introduced in Refs. 19 and 21 for the total broadening, if Γ_a, Γ_r, and Γ_{C} are separately determined. Indeed, in the SCBA theory, the self-consistent procedure is formulated for the electron Green's function $G_N(E)$, which is determined by the self-consistent pair of equations: the Dyson equation and equation for the electron self-energy. The total broadening is determined automatically, if the total self-energy is factored with $G_N(E)$, as in Eq. (17). Therefore the enhancement of scattering, due to the concentration of the density of states, proportioned to $\hbar\omega_c/\sqrt{\Gamma_a^2+\Gamma_{\mathrm{C}}^2}$ leads straightforwardly to a new and more simple equation for the total conductivity (see Sec. IV A) than equations used previously in Refs. 19 and 21.

The Coulomb broadening is important for weak magnetic fields and high electron densities, due to $\Gamma_{\mathrm{C}}\propto n^{3/4}/\sqrt{B}$. At strong magnetic fields the collision broadening dominates, since it increases with the magnetic field like $\Gamma_a\propto\sqrt{B}$.

Thus in the many-electron SCBA theory, the complicated problem of the influence of internal forces on the quantum magnetotransport of a nondegenerate 2D electron liquid becomes a matter of a single numerical factor b, which is close to unity. In principle a rigorous estimation of b can be done in a more advanced theory. At the same time, any model calculation will not be able to give a more accurate value than the simple choice $b\approx 1$, which appears to be in remarkable agreement with the linear experimental data for both the vapor and the ripplon scattering regime.

In general, Eq. (16) is actually an integral equation for $\Sigma_N(E)$, which is rather difficult to solve. We assume that in the limiting case $k_{\mathrm{B}}T\gg\Gamma$ the final result is nearly independent of the particular shape of the electron density of states (the assumption is checked for two kinds of shapes: Gaussian and semielliptic). Then for the semielliptic shape, the level

broadening can be defined as $\Gamma_N = -2\ \mathrm{Im}\Sigma_N(E_N)$ (an analogous treatment for 2D semiconductor systems was used in Ref. 30). Taking into account that $D_a^{(0)}(q,\omega)$ and $D_r^{(0)}(q,\omega)$ (at $N_q^{(r)} \gg 1$) are purely imaginary, and neglecting the mixing of the different Landau levels ($\Gamma_N \ll \hbar\omega_c$), the self-consistent equation for the Landau-level broadening can be written as

$$\Gamma_N = 2\sum_{\mathbf{q}} |J_{NN}|^2 \int \frac{d\omega}{2\pi} \mathrm{Im}G_N(E-\hbar\omega) \sum_j U_j^2 \times \mathrm{Im}D_j^{(0)}(q,\omega+\mathbf{q}\cdot\mathbf{u}) + \frac{\Gamma_{C,N}^2}{\Gamma_N}. \quad (20)$$

To solve this equation, we use the analytical approximation of Eq. (13) for $\mathrm{Im}G_N(E)$. Equation (20) describes the influence of the inelastic and nonlinear effects on the broadening of the electron density of states.

It should be additionally emphasized that, according to numerical evaluations that will be presented in Sec. IV, the main inelastic and nonlinear narrowing of $\nu(B,u)$ comes from the frequency dependence of DSF [Eq. (14)] rather than from Eq. (20). The inelastic and nonlinear changes of the Landau-level broadening appear to be small as compared to changes of the collision frequency. This explains the remarkable efficiency of the SCBA in describing our experimental data.

D. The heating effect

In order to determine the electron temperature T_e, we consider the energy-transfer rate from the electron system to vapor atoms and ripplons $\dot{P}_{\mathrm{en}}$, which can be represented in the form $\dot{P}_{\mathrm{en}} = (T_e - T)N_e\nu_{\mathrm{en}}$, where ν_{en} is the energy collision frequency. The energy balance equation can be written as

$$\frac{T_e - T}{T} = \frac{mu^2}{k_B T}\frac{\nu}{\nu_{\mathrm{en}}}\frac{\Delta N_e}{N_e}, \quad (21)$$

where ΔN_e is the number of SE in the EMP wave that absorb energy from the electric field. Equation (21) takes into account that the electron-electron collision frequency is much higher than ν_{en} and, therefore, all electrons N_e are at the same temperature T_e.

We will see that the main change of σ_{xx} caused by the cold nonlinear effect occurs for $\lambda = \sqrt{2}\hbar u/l\Gamma < 1$. Using the relation between u and λ one can find

$$\frac{T_e - T}{T} = \lambda^2 \frac{\nu}{2\nu_{\mathrm{en}}}\frac{\Gamma^2}{\hbar\omega_c k_B T}\frac{\Delta N_e}{N_e}. \quad (22)$$

For electron scattering on vapor atoms $\nu/\nu_{\mathrm{en}} \sim 0.5\times 10^{-2}$.[31] In the single-electron approximation, Γ^2 has the same magnetic field dependence as ω_c. At $T \sim 1$ K, it can be estimated that $(T_e - T)/T \sim \lambda^2 \Delta N_e/N_e$, and therefore heating can be neglected in the EMP method of measuring the SE magnetoconductivity since $\Delta N_e \ll N_e$.

In the ripplon scattering regime, the energy collision frequency is substantially lower and the heating effect should be taken into account at least for weak magnetic fields $B \sim 1$ T. The same method as described in Sec. III B yields

$$\nu_{\mathrm{en}} = \frac{1}{4\pi\rho T_e}\int_0^{2\pi}\frac{d\varphi}{2\pi}\int_0^{\infty} dq q^2 V_q^2 S_0(q, \omega_q - \mathbf{q}\cdot\mathbf{u}). \quad (23)$$

This equation is the result of one-ripplon scattering processes under the condition $\hbar\omega_q \ll k_B T$. The two-ripplon process of electron emission of short wavelength ripplons which are important in the case of $B=0$ (Ref. 32) are suppressed by the peaked structure of the electron density of states ($\Gamma \ll k_B T$) at strong magnetic fields.

IV. RESULTS AND DISCUSSIONS

A. Vapor atom scattering regime

The vapor atom scattering has the most simple form, and therefore it is instructive to start the final analysis of the cold nonlinear magnetotransport with this case. First we note that for $T > 1$ K, the energy exchanged at a collision in a fixed frame $\hbar\Delta\omega_a \approx \hbar(\mathbf{q}\cdot\mathbf{q}' + kk')/M$ (here M is the helium atom mass) can be neglected in comparison to Γ.

Before going into the details of the nonlinear analysis, we use the vapor atom scattering as a probe for the many-electron SCBA theory. For a semielliptic Landau-level shape one can find the effective collision frequency within the linear theory

$$\nu_{\mathrm{lin}}(B) = \frac{2\omega_c\Gamma_a^2}{\pi\Gamma^2 I_1(\Gamma/k_B T)}\coth\left(\frac{\hbar\omega_c}{2k_B T}\right)\times[\cosh(\Gamma/k_B T) - (k_B T/\Gamma)\sinh(\Gamma/k_B T)]. \quad (24)$$

Here $I_1(x)$ is the modified Bessel function of first order; the electron-atom interaction parameters are combined into $\Gamma_a = \hbar\sqrt{(2/\pi)\omega_c\nu_0}$, which represents the linear level broadening for pure vapor atom scattering. For the Gaussian Landau-level shape we have

$$\nu_{\mathrm{lin}}(B) = \frac{\sqrt{\pi}\omega_c\Gamma_a^2}{4\Gamma k_B T}\exp\left[-\left(\frac{\Gamma}{4k_B T}\right)^2\right]\coth\left(\frac{\hbar\omega_c}{2k_B T}\right). \quad (25)$$

Equation (25) is numerically close to Eq. (24), if $k_B T > \Gamma$. Equations (24) and (25) are many-electron extensions of the results of the single-electron theory.[3] It is important to note that here Γ originates from the real density of states, while Γ_a is the formal combination of the interaction parameters like U_a, mean vapor density n_G, and the parameter of the electron wave function $\langle z|1\rangle \propto z\exp(-\gamma_e z)$, according to $\nu_0 = (3U_a^2 n_G \gamma_e m)/8\hbar^2$. In the pure case $\Gamma = \Gamma_a$, it is usual to cancel the broadening entering the denominator of Eqs. (24) and (25) to the expense of the numerator, which hides the singular nature of the conductivity $\sigma_{xx} \propto 1/\Gamma$.

In general, we should separate the total broadening Γ from Γ_a in Eqs. (24) and (25) due to the other interactions that are present. For instance, the many-electron effect broadens additionally the Landau level, which makes $\Gamma \equiv \Gamma_{\mathrm{lin}} = \sqrt{\Gamma_a^2 + \Gamma_C^2}$. The total broadening as a function of B has a minimum whose position depends on the electron density n and T.

In the weak magnetic field range, the increase of Γ induced by the many-electron effect ($\Gamma_C \propto 1/\sqrt{B}$) is the cause for the conductivity decrease (relative to the single-electron theory result) observed in Refs. 19 and 33. It should be noted

that Eqs. (24) and (25) are valid only for rather small broadening $2\Gamma < \hbar\omega_c$, which allows one to neglect mixing of the different Landau levels. In the single-electron SCBA theory this restriction is less important, since $\Gamma_a \propto \sqrt{B}$. The restriction becomes decisive for the many-electron theory due to the rapid increase of Γ_C with a decrease of the magnetic field. Additionally, the equations are restricted by the quantum condition $\hbar\omega_c > k_B T$, since we neglected the dependence of Γ_C on the level number N.

It is instructive to compare Eq. (25) with the result of the lattice model theory introduced in Refs. 18 and 34 to describe the many-electron effect,

$$\rho_{xx}(B)/\rho_{xx}(0) = 0.15(\omega_c/\omega_p)(\hbar\omega_c/k_B T)^{3/2}, \qquad (26)$$

where $\omega_p = (2\pi e^2 n^{3/2}/m)^{1/2}$ is the plasmon frequency. In the ultra-quantum limit, the many-electron SCBA equation $\rho_{xx}(B)/\rho_{xx}(0) = \nu(B)/\nu(0)$ yields $(\hbar\omega_c)^2/(2\sqrt{\pi}\Gamma k_B T)$, which would have the same analytical behavior as Eq. (26), if the vapor-atom-induced broadening is neglected $\Gamma \to \Gamma_C$. For the numerical factor b which describes the Coulomb broadening in Eq. (18), the comparison gives $b \simeq 1.58$. The comparison of Eq. (25) with experimental data, which will be presented later, shows that this value of b overestimates the many-electron effect, and the parameter b is closer to unity.

In Refs. 19 and 21 the quantum magnetotransport was analyzed by means of the Einstein relation between the mobility and the diffusion constant, which gives

$$\sigma_{xx} = \frac{e^2 n}{m} \frac{\hbar}{2k_B T \omega_c \tau_B}. \qquad (27)$$

It is very important to establish the correct physical meaning of the so-called scattering rate in the field τ_B^{-1}. It is surely not a momentum relaxation rate $\nu(B)$, since according to the general analysis of Ref. 3, at $\omega_c \gg \nu$ we have $\sigma_{xx} \simeq e^2 n \nu(B)/m\omega_c^2$. The comparison with Eq. (27) gives $\hbar/\tau_B = 2k_B T \nu(B)/\omega_c$. In Refs. 19 and 21 $\hbar/\tau_B$ was treated as a collision broadening and combined with Γ_C to get the total broadening. The many-electron SCBA results [Eqs. (24) and (25)] show that this is true only when one kind of scatterer is present. Comparing the result of Eq. (24) with the formula based on the Einstein relation, Eq. (27), one finds

$$\frac{\hbar}{\tau_B} = \frac{8}{3\pi}\frac{\Gamma_a^2}{\Gamma} \equiv \frac{8}{3\pi}\frac{\Gamma_a^2}{\sqrt{\Gamma_a^2 + \Gamma_C^2}} \qquad (28)$$

for the semielliptic Landau-level shape. For a Gaussian shape the numerical factor $8/3\pi$ should be replaced by $\sqrt{\pi}/2$. Equation (28) shows that $\hbar/\tau_B$ can be treated as a collision broadening only for $\Gamma_C = 0$, which results into $\Gamma = \Gamma_a$. In general, $\hbar/\tau_B$ is not a collision broadening and cannot be combined with Γ_C in order to get the total broadening. According to the many-electron SCBA result, the total broadening $\Gamma = \sqrt{\Gamma_a^2 + \Gamma_C^2}$ differs from the previously used expressions $\hbar/\tau_B + \Gamma_C$,[19] and $\sqrt{(\hbar/\tau_B)^2 + \Gamma_C^2}$.[21] Therefore, the combined theoretical conductivity obtained in Refs. 19 and 21 by means of an additional self-consistent procedure for the total broadening to fit experimental data is not correct and can only be considered as an interpolation formula.

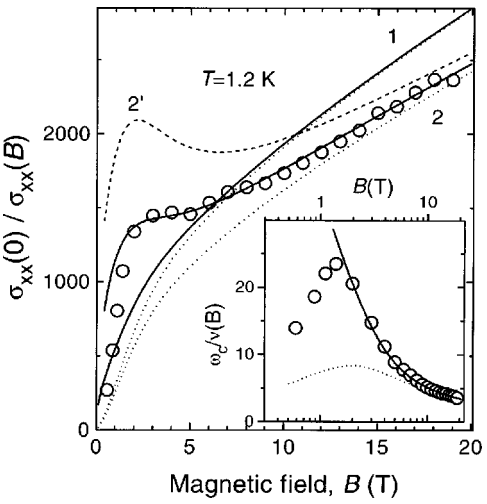

FIG. 4. The inverse conductivity $\sigma_{xx}(0)/\sigma_{xx}(B)$ vs the magnetic field B for $T = 1.2$ K. The many-electron SCBA is shown by the solid ($b = 1$) and the dashed ($b = 1.58$) curves for two electron densities: $n = 0.75 \times 10^8$ cm^{-2} (1) and $n = 3.2 \times 10^8$ cm^{-2} (2 and 2′). Dotted curves represent the extended SCBA theory.[3] Data (circles) are taken from Ref. 33. The inset shows $\omega_c/\nu(B)$ vs the magnetic field for the highest density.

The physically correct combination of the conductivity due to the many-electron effect σ_m and the single-electron conductivity σ_s can be found in a straightforward way, as follows. As mentioned in Sec. III C, there is no need for any additional self-consistent procedure once Γ_a and Γ_C are determined. We note that Eq. (28) is in accordance with the scattering rate enhancement in a magnetic field $\tau_B^{-1} \approx \nu_0 \hbar\omega_c/\Gamma$. Then, using the correct definition for $\Gamma = \sqrt{\Gamma_a^2 + \Gamma_C^2}$ and using the relations $\sigma_m \propto \Gamma_a^2/\Gamma_C$ and $\sigma_s \propto \Gamma_a$, one finds the proper equation

$$\sigma_{xx} = \frac{\sigma_s \sigma_m}{\sqrt{\sigma_s^2 + \sigma_m^2}}, \qquad (29)$$

which should be employed instead of the interpolation formulas.

As shown in Ref. 3, for low electron densities the extended single-electron SCBA perfectly describes the experimental data in a wide range of magnetic fields up to 20 T. Equations (24) and (25) of the linear many-electron SCBA theory show the way by which the Coulomb broadening and the broadening induced by vapor atom scattering should be combined in the magnetoconductivity equations. In order to find an appropriate value for the numerical factor b entering into Eq. (18), in Fig. 4 we plot the magnetic field dependence of the ratio $\sigma_{xx}(0)/\sigma_{xx}(B)$ and the experimental data of Ref. 33 for the SE conductance. The conductance is proportional to σ_{xx} with a numerical factor of order unity, which is unknown for the experiment of Ref. 33. We fix this constant to fit the data and theory at extremely strong magnetic fields ($B \simeq 20$ T), where the many-electron effect can be neglected. The magnetic field dependence of the ratio $\sigma_{xx}(0)/\sigma_{xx}(B)$ at intermediate fields $B \leqslant 5$ T appears to be very sensitive to the many-electron effect. Figure 4 shows (even qualitatively) that the numerical value $b \simeq 1.58$ found from a comparison with the lattice model theory[18,34] overes-

timates the many-electron effect (dashed curve), while the simplest choice $b=1$ leads to a perfect fit (solid curves) down to 2 T.

It should be noted that in Fig. 4, we neglected the electron-ripplon interaction, which is small for $T=1.2$ K, and we normalized the experimental and theoretical curves to $\sigma_{xx}(0)$ for pure electron-atom scattering. The inclusion of the electron-ripplon scattering gives $b\simeq 1.1$. This difference is within the experimental error of determining n and can therefore be disregarded. Still, curves normalized to the total $\sigma_{xx}(0)$ would be lower than curves of Fig. 4 by approximately a factor 1.15. This is due to the magnetic field effect on $\sigma_{xx}(0)/\sigma_{xx}(B)\propto 1/\nu(0)\nu(B)$, which multiplies the corrections to $\nu(0)$ and $\nu(B)$.

The cause of the deviation of the theoretical curve from the data for weak fields $B<1.5$ T is clearly seen in the inset of Fig. 4, where we plot the ratio $\omega_c/\nu(B)$ and the data extracted from the conductance experiment of Ref. 33 by means of the elementary relation between σ_{xx} and $\nu(B)$. The single electron theory (dotted curve) describes the transition from the classical Hall effect (sideways motion of electrons increases with B) to the abnormal Hall effect of the quantum regime where the sideways motion decreases with magnetic field. In the quantum regime, the single-electron theory gives $\nu(B)\propto B^{3/2}$, which increases faster than ω_c. The many-electron effect even increases this abnormal Hall effect: in the limiting case $\Gamma_C\gg\Gamma_a$ we would have $\nu(B)\propto\omega_c\Gamma_a^2/\Gamma_C \propto B^{5/2}$, since $\Gamma_C\propto 1/\sqrt{B}$. The solid curve represents the many-electron theory, Eq. (25), and the data both clearly show this increase. In the quantum regime, the data and the many-electron theory are in very good agreement in a wide range of magnetic fields 1.5 T$\leqslant B\leqslant$20 T, where the mixing of the different Landau levels can be neglected. For $B\leqslant 1.5$ T, the data deviates from the solid curve and shows the normal Hall effect. The reason for this behavior is that at weak fields the Landau-level broadening becomes comparable to the level separation (at $B=1.5$ T the ratio $2\Gamma/\hbar\omega_c\approx 0.7$), which restores the semiclassical nature of the magnetotransport, according to Ref. 18.

The agreement achieved between the theory and experiment proves that in the ultraquantum limit the many-electron effect mainly affects the electron density of states, which can be taken into account by the simple replacement $\Gamma \rightarrow\sqrt{\Gamma_a^2+\Gamma_r^2+\Gamma_C^2}$ in the final equations of the extended SCBA.

Since the experimental data of the Carbino technique might be affected by spurious effects, it is very important for the final data to satisfy a simple physical behavior, which follows from the theoretical analysis. We cannot use the data of Ref. 19 as a probe, since they do not satisfy the required limiting behavior $\sigma_{xx}(0)/\sigma_{xx}(B)$ at strong fields. The many-electron curves and the data sets for different densities should cross at $B\leqslant 7$ T under saturation condition for the holding electric field, $E_\perp=2\pi en$, due to the holding field dependence of the electron wave function. One easily finds that the strong magnetic field asymptote of the ratio $\sigma_{xx}(0)/\sigma_{xx}(B)\propto 1/[\nu_0\nu(B)]\propto\gamma_e^{-3/2}(E_\perp)$ depends on n. Therefore, each many-electron curve has its own single-electron curve as an asymptote at strong magnetic fields. The increase of $E_\perp$ with the electron density reduces the strong magnetic field asymptote, while the many-electron effect increases the weak field part of the curves. This results in a crossing of the many-electron curves, as is seen in Fig. 4. The inclusion of the electron-ripplon interaction increases this effect. In Ref. 19, the data plots $\sigma_{xx}(0)/\sigma_{xx}(B)$ for different densities do not cross but behave like they have parallel asymptotes at strong magnetic fields, which is in contradiction with the simple physical requirement mentioned above. Regarding the new data of Ref. 21, they are in contradiction with even a more simple rule, namely, that experimental plots for $1/\sigma_{xx}(B)$ should decrease with the electron density n in the limit of strong magnetic fields, due to $\sigma\propto n$.

We start our nonlinear analysis with the Landau-level broadening equation. As mentioned above, the Coulomb correction Γ_C does not depend on u [except for the weak indirect dependence due to the heating effect taken into account by $T_e(u)$], since it is caused by the fluctuating field of the electrons, which are at rest in the center-of-mass frame. On the other hand the vapor atom gas moves with the drift velocity $-\mathbf{u}$, which makes the vapor atom contribution to the level broadening dependent on u. The effect can be easily described, if we take into account that

$$D_a^{(0)}(q,\omega)=-2\pi i\sum_k |\eta_k|^2\sum_{\mathbf{K}'} N_{\mathbf{K}'}^{(a)}\delta(\omega+\Delta\omega_a). \quad (30)$$

For the semielliptic shape Eqs. (20) and (30) yield

$$\Gamma^2=\Gamma_a^2\frac{1}{2\pi}\int_0^{2\pi}d\varphi\int e^{-x}\sqrt{1-\lambda^2(\Gamma_{\rm lin}^2/\Gamma^2)x\cos^2(\varphi)}\,dx + \Gamma_C^2, \quad (31)$$

where $\Gamma_{\rm lin}=\sqrt{\Gamma_a^2+\Gamma_C^2}$ is the total linear broadening, $\lambda=\sqrt{2}\hbar u/l\Gamma_{\rm lin}\simeq\sqrt{2}eE_\parallel l/\Gamma_{\rm lin}$ is the nonlinear parameter.

We solve Eq. (31) numerically. Still, it is instructive to use a Gaussian Landau-level shape in order to reveal the nonlinear narrowing of Γ in an analytical form. In this case, the self-consistent equation reduces to

$$\Gamma^2=\frac{\Gamma_a^2\Gamma}{\sqrt{\Gamma^2+4\hbar^2u^2/l^2}}+\Gamma_C^2, \quad (32)$$

which is a cubic equation and which can be solved analytically. In the limit $\Gamma_C\ll\Gamma_a$, valid for strong magnetic fields or low electron densities, the solution is of a very simple form:

$$\Gamma^2\simeq\sqrt{\Gamma_a^4+\left(\frac{2\hbar^2u^2}{l^2}\right)^2}-\frac{2\hbar^2u^2}{l^2}, \quad (33)$$

which shows clearly the effect of the drift velocity on the level broadening. The first term describes the way by which the drift-time duration $\tau_{\rm dr}=l/u\sqrt{2}$ is combined with the linear lifetime $\hbar/\Gamma_a$. The second term in Eq. (33) provides the required physical behavior of Γ in the limiting case $\tau_{\rm dr}\ll\hbar/\Gamma_a$: there is no level broadening in the single-electron theory without vapor atom scattering ($\Gamma_a^2\rightarrow 0$).

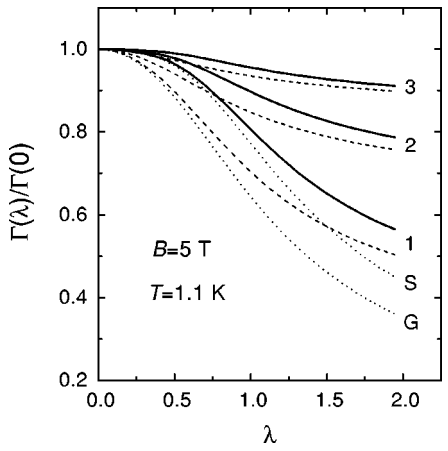

FIG. 5. The Landau-level broadening as a function of the nonlinear parameter $\lambda=\sqrt{2}\hbar u/l\Gamma_{\rm lin}$ for three electron densities: 0.5×10^8 cm^{-2} (1), 2×10^8 cm^{-2} (2), and 5×10^8 cm^{-2} (3). Solid curves represent the many-electron SCBA with a semielliptic level shape; dashed curves are from a solution of Eq. (32) for the Gaussian shape. Dotted curves represent the solution of the single-electron theory for the semielliptic (S) and the Gaussian (G) shapes as described in the text.

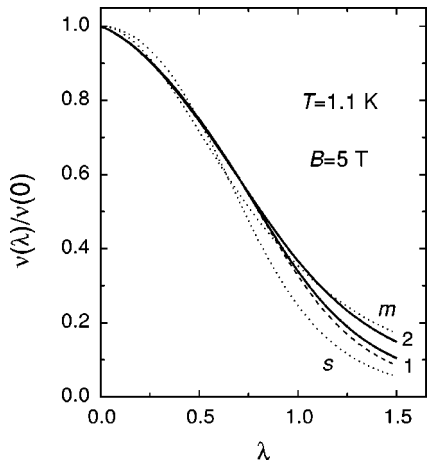

FIG. 6. The normalized effective collision frequency vs the nonlinear parameter λ for two electron densities: 0.5×10^8 cm^{-2} (1), and 2×10^8 cm^{-2} (2) for the many-electron SCBA (solid), and the single-electron theory (dashed). Dotted curves represent the results of the single-electron approximation (s) and for the extreme many-electron limit, $\Gamma_C\gg\Gamma_a$, (m) for a Gaussian Landau-level shape.

The results of a numerical evaluation of Eq. (31) are shown in Fig. 5 for three electron densities (solid curves). The level broadening becomes less dependent on the nonlinear parameter λ with increasing electron density, which is caused by the many-electron effect. The results of the Gaussian approximation (dashed curves) for $\Gamma(\lambda)$ behave in a similar way, but they are shifted towards the range of smaller λ. The reason is that this shape for the Landau level is not appropriate for the self-consistent equation that is used, due to the shape factor $\sqrt{\pi/2}$. Correcting the nonlinear parameter λ by this factor shifts the dashed curves close to the solid curves, but this procedure is introduced only to show that the result does not depend significantly on the real Landau-level shape. The linear broadening of the Gaussian density of states found in the lowest-order cumulant approach[28] is the same as the broadening of the SCBA. Therefore, the solution given by Eq. (31) is the most appropriate one. Moreover, as will be shown below, the main nonlinear reduction of the effective collision frequency is nearly independent of the nonlinear change of Γ.

According to Eqs. (11) and (14), the effective collision frequency of the cold nonlinear effect ($T_e\simeq T$) becomes

$$\frac{\nu(\lambda)}{\nu_{\rm lin}}=\frac{\Gamma_{\rm lin}}{\Gamma}\frac{1}{\pi}\int_0^{2\pi}d\varphi\cos^2(\varphi)\int_0^{\infty}dx x e^{-x}\times Y_S\left(\lambda\frac{\Gamma_{\rm lin}}{\Gamma}\sqrt{x}\cos(\varphi)\right). \tag{34}$$

As pointed out in Sec. II B, it does not matter which representation is used $Y_S(y)$ or $Y_G(y)$, since they are very close. For the Gaussian shape, the nonlinear collision frequency can be found in analytical form

$$\frac{\nu(\lambda)}{\nu_{\rm lin}}=\frac{\Gamma_{\rm lin}}{\Gamma}\left[1+\lambda^2\frac{\Gamma_{\rm lin}^2}{\Gamma^2}\right]^{-3/2}. \tag{35}$$

Here the total broadening Γ is a function of λ. It is instructive to consider two extreme cases corresponding to the single-electron approximation [$\Gamma(\lambda)$ is determined by Eq. (33)] and approximation $\Gamma_C\gg\Gamma_a$ or $\Gamma(\lambda)=$const. In the first case,

$$\frac{\nu(\lambda)}{\nu_{\rm lin}}=\frac{\sqrt{1+\lambda^4}-\lambda^2}{(1+\lambda^4)^{3/4}}. \tag{36}$$

The approximation $\Gamma(\lambda)=$const yields the more simple form $\nu(\lambda)/\nu_{\rm lin}=(1+\lambda^2)^{-3/2}$. Both these extreme analytical equations are shown in Fig. 6 by the dotted curves (s and m). First, it should be noted that both curves are remarkably close to each other, which supports the approximations used in Ref. 11. Any many-electron nonlinear curve, within the Gaussian approximation, will be situated between the curves s and m. Secondly, the sharp nonlinear narrowing of ν (Fig. 6) is more important than the rather weak narrowing of $\Gamma(\lambda)/\Gamma_{\rm lin}$, which is also suppressed by the many-electron effect, according to Fig. 5.

The results of a numerical evaluation of Eq. (34) for the semielliptic shape are shown in Fig. 6 by the solid (many-electron theory) and dashed (single-electron approximation) curves. These results additionally prove the universal behavior of the ratio $\nu(\lambda)/\nu_{\rm lin}$ at $\lambda<1$, where the main nonlinear narrowing occurs. Of course, the universal behavior of $\nu(\lambda)/\nu_{\rm lin}$ does not imply that the nonlinear effect is insensitive to the many-electron effect, since λ depends on $\Gamma_{\rm lin}$, which contains the Coulomb correction Γ_C. Therefore, the dependence of the SE conductivity on the driving electric field is affected by the many-electron fluctuating field, as well as the magnetic field dependence of the critical drift velocity.

It should be emphasized that the dotted curves in Fig. 6 are plotted for the Gaussian Landau-level shape, which was used for calculating both ν and Γ. This shape is surely not appropriate for the self-consistent equation, as it was discussed above. Nevertheless, the dotted and solid curves are

close, which proves that the results do not depend much on the specific Landau-level shape used. The simple analytical form of the nonlinear effect allows one to obtain direct experimental knowledge of the Landau-level broadening for the strongly correlated 2D electron liquid.

B. Electron-ripplon scattering regime

The low-temperature regime of the SE magnetotransport ($T<0.7$ K) is more difficult to analyze than the vapor gas scattering regime, due to the complicated form of the electron-ripplon coupling V_q.[23] At the same time, this limiting case is the most convenient one for experimental observation of the cold quantum nonlinear magnetotransport phenomena, since the level broadening decreases with lowering T, and therefore much weaker driving electric fields are required to reach the condition $\lambda \sim 1$.

To describe ripplon-induced broadening we use the relation

$$\mathrm{Im}D_r^{(0)}(q,\omega) = -\pi(2N_q^{(r)}+1)[\delta(\omega-\omega_q)+\delta(\omega+\omega_q)], \tag{37}$$

which is similar to Eq. (30) for the vapor atom scattering. Assuming the capillary dispersion $\omega_q \propto q^{3/2}$, one finds

$$\Gamma^2 = \Gamma_C^2 + \frac{\Lambda^2 k_B T}{\pi\alpha l^4}\int_0^{2\pi}\frac{d\varphi}{2\pi}\int W^2(x)e^{-x} \times \sqrt{1-\frac{\Gamma_{\mathrm{elas}}^2}{\Gamma^2}[\delta x^{3/4}+\lambda\sqrt{x}\cos(\varphi)]^2}\frac{dx}{x}, \tag{38}$$

where the second integral is limited to the positive x range for which the square root is real; $\delta = \hbar\omega_0/\Gamma_{\mathrm{elas}}$ is the inelastic parameter [$\omega_0^2 = \alpha(\sqrt{2}/l)^3/\rho$] and $\lambda = \sqrt{2}\hbar u/\Gamma_{\mathrm{elas}} l$ is the nonlinear parameter, $\Gamma_{\mathrm{elas}} = \sqrt{\Gamma_r^2+\Gamma_C^2}$ is the total elastic broadening,

$$W(x) = xw\left(\frac{x}{2\gamma_e^2 l^2}\right) + \frac{eE_\perp l^2}{\Lambda}, \quad \Lambda = \frac{e^2(\epsilon_{\mathrm{He}}-1)}{4(\epsilon_{\mathrm{He}}+1)},$$

$$w(y) = -\frac{1}{1-y} + \frac{1}{(1-y)^{3/2}}\ln\left[\frac{1+\sqrt{1-y}}{\sqrt{y}}\right], \tag{39}$$

ϵ_{He} is the dielectric constant of liquid helium; $E_\perp$ is the holding electric field. Equation (38) represents the self-consistent equation for the Landau-level broadening, which is to be solved numerically.

According to Eqs. (11) and (14), the nonlinear effective collision frequency can be written as

$$\nu^{(r)} = \frac{4m^2\Lambda^2\omega_c^3 T}{3\pi^2\alpha\hbar^2\Gamma T_e}\int_0^{2\pi}\frac{d\varphi}{\pi}\cos^2(\varphi)\int_0^\infty dx W^2(x)e^{-x} \times Y_S\left(\frac{\Gamma_{\mathrm{elas}}}{\Gamma}[\delta x^{3/4}+\lambda\sqrt{x}\cos(\varphi)]\right). \tag{40}$$

Equation (40), as well as Eq. (38) for the level broadening, incorporates both the inelastic and nonlinear effects on equal footing, which agrees with the physical concept of the cold nonlinear magnetotransport as a nonlinear breakdown of the elastic approximation discussed in the Introduction.

In the quasielastic limiting case ($\hbar\omega_q \ll \Gamma$) of linear magnetotransport ($\lambda \ll 1$), the ripplon-induced broadening and the effective collision frequency can be written as follows:

$$\Gamma_r^2 = \frac{\Lambda^2 k_B T}{\pi\alpha l^4}\int_{x_0}^\infty W^2(x)e^{-x}dx/x,$$

$$\nu_0^{(r)}(B) = \frac{4m^2\Lambda^2\omega_c^3}{3\pi^2\alpha\hbar^2\Gamma_{\mathrm{elas}}}\int_0^\infty W^2(x)e^{-x}dx. \tag{41}$$

The effective collision frequency of Eq. (41) shows the singular nature of the elastic magnetotransport $\nu_0(B) \propto 1/\Gamma_{\mathrm{elas}}$. The lower limit x_0 of the integral that enters the level broadening equation is introduced in order to cut off the logarithmic singularity of the $E_\perp^2$ term, which appears for the capillary spectrum. Of course, there is no singularity when the real ripplon spectrum is used, which has the gravity-wave behavior $\omega \propto q^{1/2}$ for $q \to 0$. For the case of non-zero electron density, the cutoff at wave vectors $q \approx \sqrt{n}$, where the many-electron effect screens the electron-ripplon interaction, is more important. Still, in the low-temperature limit, low electron densities are required for the system to be in a liquid state, and this singular term is usually much smaller than the polarization term of the electron-ripplon interaction.

The field dependence of $\nu_0^{(r)}$ as well as Γ_r is hidden, due to the complicated form of the interaction potential $W(x)$. It is possible to reveal it in a qualitative way, if we take into account that $w(y)$ is numerically close to $1/(3\sqrt{y})$, which is also supported by the temperature dependence of the zero-field mobility $\mu \propto 1/T$, observed experimentally.[35,36] At low temperatures $T \sim 0.3$ K the electron density should be rather small $n \leq 4\times 10^7$ cm to avoid the Wigner solid transition, which allows one to neglect the $E_\perp$-dependent terms in the integrals over x. In this case, we have $W^2 \propto 1/B$ and consequently $\Gamma_r \propto \sqrt{BT}$. In the single-electron treatment, it yields $\nu_0^{(r)}(B) \propto B^{3/2}/\sqrt{T}$ or $\sigma_{xx} \propto 1/\sqrt{BT}$. This temperature and field dependencies of σ_{xx} are in agreement with the results of the more sophisticated single-electron quasielastic theory (Saitoh[9]). More detailed comparison shows that the main difference between the theory of Ref. 9 and our results is just the difference of averaging of the interaction potential $W^2(x)$ by means of dimensionless integrals in the equations for $\nu_0^{(r)}(B)$ and Γ_r^2. For instance, the corresponding integral for Γ_r^2 is of the form $\int_0^\infty W^2(x)e^{-x}dx$, which is more suitable for high electron densities due to the analytical behavior at small x. In the case of high electron densities, the $E_\perp^2$ term of the corresponding integral, $(eE_\perp)^2 l^4/\Lambda^2$, can be used in Eq. (41) as an approximation instead of the logarithmically divergent term. At low electron densities employed here and $B > 2$ T, both kinds of averaging give very close results for the SE conductivity (within 13% accuracy).

In the opposite limiting case $\Gamma_C \gg \Gamma_r$, we have $\Gamma \propto \sqrt{T/B}$, which results in $\nu_0^{(r)}(B) \propto \omega_c^2\sqrt{B/T}$ or $\sigma_{xx} \propto \sqrt{B/T}$, and which

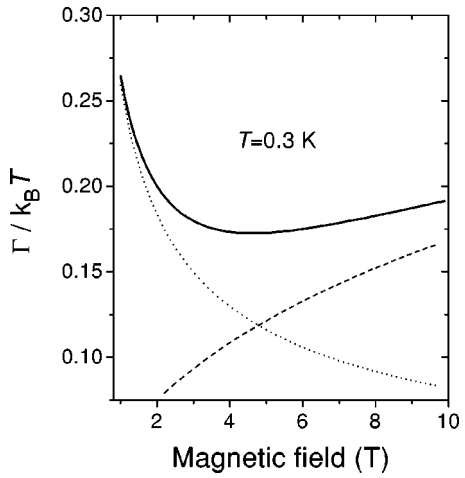

FIG. 7. The Landau-level broadening vs the magnetic field for $n=3.5\times10^7$ cm^{-2}. We show the results of the many-electron SCBA (solid), the single-electron SCBA (dashed), and the approximation $\Gamma=\Gamma_C$ (dotted).

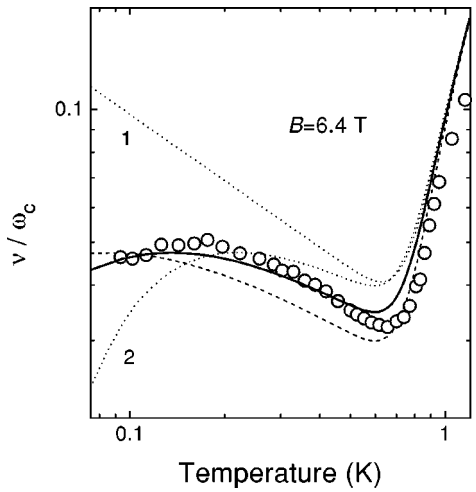

FIG. 8. Temperature dependence of the ratio ν/ω_c for $n=3.5\times10^7$ cm^{-2}. The many-electron SCBA is shown by the solid ($b=1$) and the dashed ($b=1.58$) curves. Dotted curves show the elastic many-electron theory (1) and the single-electron inelastic SCBA (2). Data are from the EMP damping coefficient using the elementary relation between σ_{xx} and ν.

exhibits field and temperature dependencies consistent with the results of the many-electron theory of Dykman and Khazan (DK).[10] Therefore we can conclude that the approach of the DK theory is physically equivalent to the Born approximation in which the broadening of the electron density of states is caused by the mutual Coulomb interaction only (i.e., $\Gamma=\Gamma_C$), while the broadening induced by ripplons Γ_r is neglected. It should be emphasized that in the ultraquantum limit, Γ_r cannot be neglected, since it increases with B, while $\Gamma_C\propto1/\sqrt{B}$ decreases. Still, it is instructive to note that formally in the limiting case $\Gamma\to\Gamma_C$ and for $n\leqslant4\times10^7$ cm, both extended SCBA and DK theories agree on a 6% accuracy level within a wide range of magnetic fields, if the absolute value of the Coulomb broadening parameter b is fixed to 1.58, according to the comparison made for the vapor atom scattering version of the DK theory.[18,34]

In the intermediate regime $\Gamma_r\sim\Gamma_C$ the total broadening as a function of B is plotted in Fig. 7 and exhibits a minimum. Since the dependencies $\Gamma_r\propto\sqrt{B}$ and $\Gamma_C\propto1/\sqrt{B}$ are rather weak, we conclude that in the intermediate case $\Gamma(B)\approx$const. This yields $\nu(B)\propto B^2$ and $\sigma_{xx}(B)\approx$const in agreement with recent measurements of Ref. 4. At the same time, the temperature dependence $\sigma_{xx}\propto1/\sqrt{T}$ is quite universal for the quasielastic theories.

At strong magnetic fields, the temperature dependence of the magnetoconductivity is crucially affected by the inelastic effect, which can serve as an additional probe for the Coulomb broadening and for the parameter b of the ultraquantum limit. The results of our numerical evaluation of the equations for Γ and ν are shown in Fig. 8, where the temperature dependence of the ratio ν/ω_c, which is proportional to SE magnetoconductivity, is shown. Note that the elastic approach (dotted curve 1) cannot explain the experimental data as found by our EMP damping method. At the same time, the single-electron inelastic theory (dotted curve 2) strongly deviates from the data at low temperatures. The inclusion of the Coulomb correction Γ_C with $b=1$ into the inelastic equations for the level broadening and effective collision frequency (solid curve) gives the best fit, in accordance with the results presented in Sec. IV A for the vapor atom scattering regime. The numerical value estimated from the many-electron theory of Refs. 18,34, $b=1.58$ (dashed curve) leads to a different temperature dependence for $T<0.25$ K, which is caused by an overestimation of the Coulomb broadening. Therefore, we found that a comparison with different experimental data in independent scattering regimes leads to the same value for the Coulomb broadening parameter $b\simeq1$, in accordance with our previous estimations[4]. Thus, we will use this value of $b=1$ in our nonlinear analysis.

In Fig. 8, the maximum reduction of the effective collision frequency caused by the inelastic effect (solid curve) reaches 64%. At the same condition, the relative narrowing of the Landau-level broadening with regard to the elastic broadening is substantially smaller (18%).

In the nonlinear regime, the effective collision frequency narrows due to both the cold nonlinear effect and the heating $\nu\propto1/T_e$, according to Eq. (40). In our nonlinear analysis of the ripplon scattering regime, we use the energy balance equation [Eq. (22)] and the energy relaxation rate of Eq. (23) to determine the electron temperature T_e as a function of the nonlinear parameter λ. The results of our numerical evaluation of the effective collision frequency as a function of the input potential V_{in} and the experimental data are shown in Fig. 9. The different theoretical curves are plotted under the assumption that the drift velocity u and the parameter λ are proportional to V_{in}. Since the exact value of the driving electric field is unknown in the EMP experiment, the proportionality factor between λ and V_{in} is fixed at one experimental point. Dotted curves represent the results for the pure cold nonlinear effect (1) and the pure heating case (2). As is seen, the cold nonlinear effect dominates the heating effect for the chosen value of the magnetic field. The solid curve (many-electron SCBA, with $b=1$), which takes into account both of these effects, is in good agreement with the data found from the EMP damping. At the same time, the single-electron theory (dashed curve) deviates substantially from the experimental results.

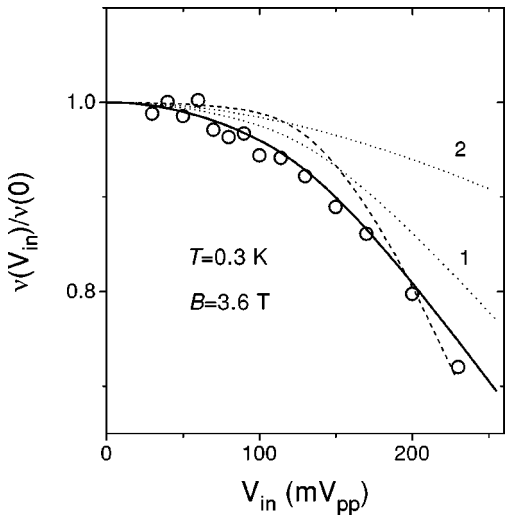

FIG. 9. The effective collision frequency vs the input voltage for the same electron density as in Fig. 5: the many-electron SCBA (solid curve) and the single-electron approximation (dashed curve). Dotted curves represent the pure cold nonlinear effect (1) and the pure heating effect (2) as described in the text. Data are obtained from the EMP damping coefficient.

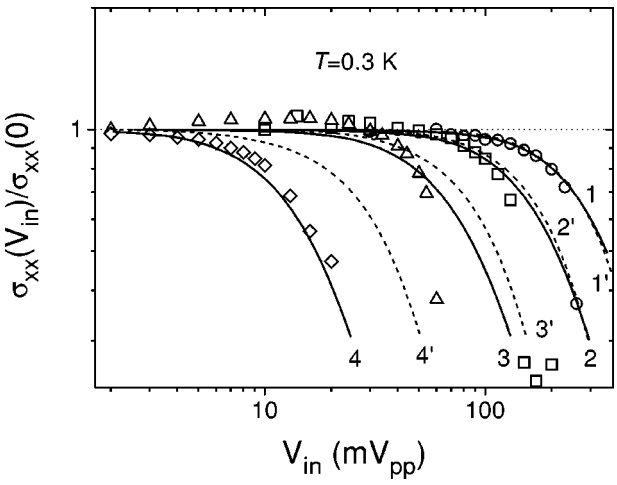

FIG. 10. The SE magnetoconductivity vs the input voltage for four values of the magnetic field: 3.6 T (circles, curves 1 and 1′), 2.7 T (squares, curves 2 and 2′), 1.8 T (triangles, curves 3 and 3′), and 0.91 T (diamonds, curves 4 and 4′). Solid curves represent the many-electron SCBA theory. Dashed curves are plotted neglecting the heating effect.

As we already mentioned, it is difficult to establish a strict numerical relation between the nonlinear parameter λ and the input potential $V_{\rm in}$. Nevertheless it is possible to reveal the magnetic field dependence of the proportionality factor. According to Eqs. (4) and (5), under resonance conditions we have $E_{\parallel} \propto \sigma_{yx}(B) V_{\rm in}/\sigma_{xx}(B)$. Therefore, the nonlinear parameter becomes

$$\lambda \propto V_{\rm in} \frac{l}{B \sigma_{xx} \Gamma_{\rm elas}}. \tag{42}$$

In the qualitative analysis we did for the linear transport regime we found $\sigma_{xx}(B)\Gamma(B) \approx$ const, which leads to the approximate relation $\lambda \propto V_{\rm in} B^{-3/2}$, which is close to the experimental one, $V_{\rm in} B^{-2} \approx$ const. We attribute the difference to the heating effect, which becomes more important with decreasing magnetic field. The results of a numerical calculation by means of Eq. (40) are shown in Fig. 10. The many-electron nonlinear theory (solid curve) shifts into the range of weaker $V_{\rm in}$ with decreasing magnetic field. The results for the pure cold nonlinear effect are shown by the dashed curves. Here the proportionality constant between the left and right sides of Eq. (42) is fixed at $B = 6.4$ T (separately for solid curve 1 and dashed curve 1′) and remains the same for all other magnetic fields. The shift between the solid and the dashed curves is caused by the heating effect.

Figure 10 shows that the many-electron SCBA describes quite effectively the nonlinear narrowing of the EMP damping coefficient and the dependence of the SE magnetoconductivity on the amplitude of the input voltage $V_{\rm in}$. According to the results of Sec. II, the theoretical curves in this figure are only strictly valid for small nonlinearities, since σ_{xx} which enters Eq. (42) is actually a function of λ. For small λ it is possible to use the linear relation between λ and $V_{\rm in}$. The decrease of σ_{xx} with λ sharply increases the effective driving electric field, which is the cause of the rapid decrease of the experimental data with $V_{\rm in}$, if the nonlinear change exceeds 30%.

V. CONCLUSION

We have investigated the nonlinear quantum magnetotransport phenomena of a nondegenerate 2D electron liquid on the surface of liquid helium. It is shown that there is a physically interesting regime where the nonlinear decrease of the EMP damping coefficient, and σ_{xx} as functions of the input voltage, is due to the singular nature of the 2D electron system in a magnetic field. This cold quantum nonlinear effect appears to be dominant at strong magnetic fields. For weak magnetic fields, $B \leqslant 1$ T, this effect is of the same importance as the usual heating effect.

To describe the nonlinear quantum magnetotransport, we introduced the many-electron SCBA theory, in which the mutual Coulomb interaction broadens the Landau levels in addition to the collision broadening produced by scatterers Γ_s. In the linear regime, this approach reproduced the results of the single-electron theory[9] and the many-electron DK theory[10] in the opposite limiting cases with regard to the parameter Γ_C/Γ_s ($\Gamma_C/\Gamma_s = 0$,[9] and $\Gamma_C/\Gamma_s = \infty$,[10] respectively). The theory describes the available linear magnetoconductivity data in both the vapor atom and the ripplon scattering regimes. The nonlinear magnetoconductivity data obtained here from the EMP damping coefficient for the ripplon dominated scattering regime are shown to be in good (even quantitative) agreement with the many-electron SCBA theory.

ACKNOWLEDGMENTS

This work was partly supported by a Grant-in-Aid for Scientific Research from Monbusho, a Toray Science and Technology Grant, the INTAS-93-1495-ext project, and the Flemish Science Foundation.

[1] K. von Klitzing, G. Dorda, and M. Pepper, Phys. Rev. Lett. **45**, 494 (1980).
[2] D. C. Tsui, H. L. Stormer, and A. C. Gossard, Phys. Rev. Lett. **48**, 1559 (1982).
[3] P. J. M. Peters, P. Scheuzger, M. J. Lea, Yu. P. Monarkha, P. K. H. Sommerfeld, and R. W. van der Heijden, Phys. Rev. B **50**, 11 570 (1994).
[4] Yu. P. Monarkha, S. Ito, K. Shirahama, and K. Kono, Phys. Rev. Lett. **78**, 2445 (1997).
[5] R. Kubo, S. J. Miyake, and N. Hashitsume, Solid State Phys. **17**, 269 (1965).
[6] T. Ando and Y. Uemura, J. Phys. Soc. Jpn. **36**, 959 (1974).
[7] Yu. P. Monarkha, K. Shirahama, and K. Kono, Low Temp. Phys. **23**, 472 (1997).
[8] Yu. P. Monarkha, Low Temp. Phys. **19**, 530 (1993).
[9] M. Saitoh, Solid State Commun. **52**, 63 (1984).
[10] M. I. Dykman and L. S. Khazan, Zh. Éksp. Teor. Fiz. **77**, 1488 (1979) [Sov. Phys. JETP **50**, 747 (1979)].
[11] Yu. P. Monarkha and F. M. Peeters, Europhys. Lett. **34**, 611 (1996).
[12] S. Ito, K. Shirahama, and K. Kono, J. Phys. Soc. Jpn. **66**, 533 (1997).
[13] P. K. H. Sommerfeld, R. W. van der Heijden, and A.T.A.M. de Waele, in Proceedings of the 21st International Conference on Low Temperature Physics, Prague, Czechoslovak, 1966 [J. Phys. (Paris) **46**, Suppl. S1, p. 319 (1996)].
[14] D. B. Mast, A. J. Dahm, and A. L. Fetter, Phys. Rev. Lett. **54**, 1706 (1985).
[15] D. C. Glattli, E. Y. Andrei, G. Deville, J. Poitrenaud, and F. I. B. Williams, Phys. Rev. Lett. **54**, 1710 (1985).
[16] V. A. Volkov and S. A. Mikhailov, in *Modern Problems in Condensed Matter Sciences*, edited by V. M. Agranovich and A. A. Maradudin (North-Holland, Amsterdam, 1991) Vol. 27.2, Chap. 15, p. 855.
[17] I. L. Aleiner and L. I. Glazman, Phys. Rev. Lett. **72**, 2935 (1994).
[18] M. I. Dykman, M. J. Lea, P. Fozooni, and J. Frost, Phys. Rev. Lett. **70**, 3975 (1993).
[19] M. J. Lea, P. Fozooni, P. J. Richardson, and A. Blackburn, Phys. Rev. Lett. **73**, 1142 (1994).
[20] V. B. Shikin, JETP Lett. **47**, 555 (1988).
[21] M. J. Lea, P. Fozooni, A. Kristensen, P. J. Richardson, K. Djerfi, M. I. Dykman, C. Fang-Yen, and A. Blackburn, Phys. Rev. B **55**, 16 280 (1997).
[22] W. Cai, X. L. Lei, and C. S. Ting, Phys. Rev. B **31**, 4070 (1985).
[23] Yu. P. Monarkha and V. B. Shikin, Sov. J. Low Temp. Phys. **8**, 279 (1982).
[24] P. W. Adams and M. A. Paalanen, Phys. Rev. B **37**, 3805 (1988); **38**, 5064(E) (1988).
[25] R. W. van der Heijden, M. C. M. van de Sanden, J. H. G. Surewaard, A. T. A. M. de Waele, H. M. Gijsman, and F. M. Peeters, Europhys. Lett. **6**, 75 (1988).
[26] H. Totsuji, Phys. Rev. B **22**, 187 (1980).
[27] H. Fukuyama, Y. Kuramoto, and P. M. Platzman, Phys. Rev. B **19**, 4980 (1979).
[28] R. R. Gerhardts, Surf. Sci. **58**, 227 (1976).
[29] T. Ando, J. Phys. Soc. Jpn. **37**, 622 (1974).
[30] D. R. Leadley, R. J. Nicholas, W. Xu, F. M. Peeters, J. T. Devreese, J. Singleton, J. A. A. J. Perenboom, L. van Bockstal, F. Herlach, C. T. Foxon, and J. J. Harris, Phys. Rev. B **48**, 5457 (1993).
[31] M. Saitoh, J. Phys. Soc. Jpn. **42**, 201 (1977).
[32] Yu. P. Monarkha, Sov. J. Low Temp. Phys. **4**, 515 (1978).
[33] P. Scheuzger, J. Neuenschwander, W. Joss, and P. Wyder, Physica B **194-196**, 1231 (1994).
[34] M. I. Dykman, J. Phys. C **15**, 7397 (1982).
[35] A. S. Rybalko, Yu. Z. Kovdrya, and B. N. Esel'son, Pis'ma Zh. Éksp. Teor. Fiz. **22**, 569 (1975) [JETP Lett. **22**, 280 (1975)].
[36] R. Mehrotra, C. J. Guo, Y. Z. Ruan, D. B. Mast, and A. J. Dahm, Phys. Rev. B **29**, 5239 (1984).